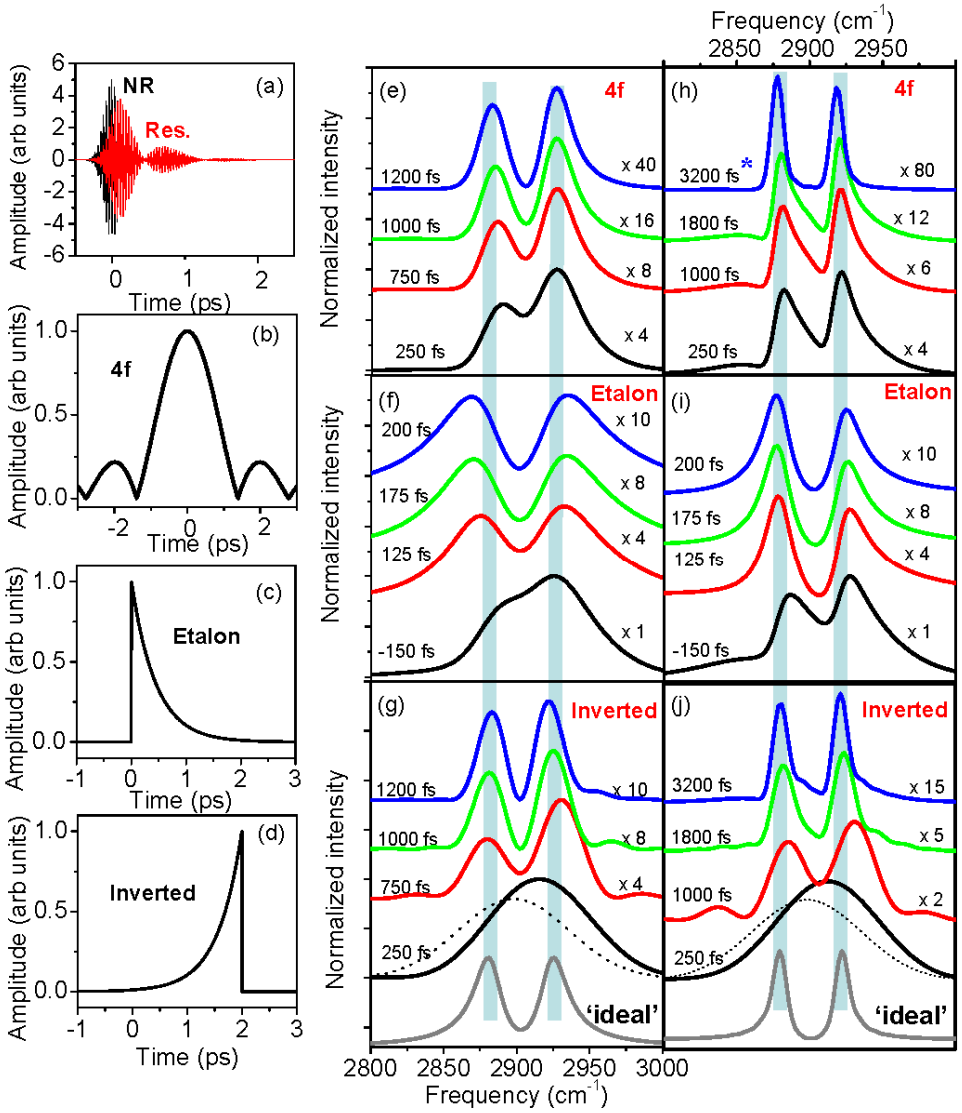

Fig. 1. Schematic representation of time domain pictures for BB-SFG and the effect of ps pulse shape of the SFG spectra. (a) resonant (red) and nonresonant (black) contributions to the oscillating first order polarization $P^{(1)}(t)$. The ps visible pulse shapes, each with 24 cm^{-1} linewidth are shown: (b) the time-symmetric pulse from a 4f pulse shaper; (c) the time-asymmetric pulse shape from a Fabry-Perot étalon; (d) the 'inverted' time-asymmetric pulse shape obtained via second harmonic generation in a long $LiNbO_3$ crystal. The BB-SFG spectra were calculated for two IR transitions, centered at 2880 cm^{-1} and 2920 cm^{-1}, in the presence of a large (5 ×) NRB having a phase shift of $\pi/2$. The 150 fs IR laser pulse spectrum was centered at 2900 cm^{-1}. The left column, (e), (f) and (g) shows results for a ps visible pulse of 24 cm^{-1} FWHM and resonance linewidths of 30 cm^{-1} FWHM. The right column, (h), (i) and (j) shows results for a narrow ps visible pulse of 10 cm^{-1} FWHM and narrow resonance linewidth of 12 cm^{-1}. The effects of the shaped, delayed ps visible pulse are shown as a function of delay for: the 4f pulse shape in (e) and (h); the etalon pulse shape in (f) and (i); the inverted pulse shape in (g) and (j). The magnification relative to the short time (250 fs) response of the inverted pulse (solid black line in (g) and (j)) are given on the right of each spectrum. It can be seen that the signal levels decreases rapidly as a function of delay. The fs IR pulse spectrum is shown as a dashed line in (g) and (j). For comparison, 'ideal' spectra (without NRB) for both computed examples are given in (g) and (j). For discussion, see the text.

#126129- $15.00USD Received 29 Mar 2010; revised 29 Apr 2010; accepted 6 May 2010; published 14 May 2010

2. Theory

The BB-SFG scheme requires narrowband ps visible and fs IR pulses, the former determining the spectral resolution. In a time domain representation of a BB-SFG experiment, the fs IR pulse induces an oscillating time dependent first order polarization

$$P^{(1)}(t) = P_{NR}^{(1)}(t) + P_{R}^{(1)}(t) \tag{1}$$

where $P_{NR}^{(1)}(t)$ is the instantaneous electronic response of the system to the electric field of the IR pulse and is only present during the IR pulse. The second term, $P_{R}^{(1)}(t)$, the free-induction decay (FID), contains the oscillating vibrational coherences induced by the resonant response of the system and has a decay lifetime related to the inverse linewidths of the IR transitions [8,11]. In a time domain SFG measurement, the envelope of the oscillating coherences can be measured by upconverting the first order polarization with a delayed ultrashort visible pulse. In a frequency domain BB-SFG measurement, it is a ps visible pulse which upconverts the oscillating first order polarization to the second order field $P_{SFG}^{(2)}(t)$ which is subsequently measured as the SFG power spectrum $P_{SFG}^{(2)}(\omega)$ in a spectrometer.

In a mixed frequency and time domain representation, BB-SFG can be formulated as follows. The time domain molecular response function is given by [8]

$$S(t') = \left\{ A_{NR} \exp(i\varphi_{NR})\delta(t) - i\theta(t')\sum_{j} B_j \Gamma_j \exp(-\Gamma_j t' - i\omega_j t') \right\} \tag{2}$$

The first term represents the instantaneous nonresonant contribution, the second the resonant vibrational coherences, assuming a set of homogeneously broadened Lorentzian line shapes. The factors A_{NR} and φ_{NR} are the amplitude and phase of the nonresonant response, with respect to the vibrational coherence. For the resonant response term, B_j, Γ_j and ω_j are the Lorentzian amplitudes, line widths and central frequencies, respectively, of the IR transitions and θ is the Heaviside step function. The short IR pulse interacts with the system and induces the first order polarization $P^{(1)}(t)$,

$$P^{(1)}(t) = \int_{-\infty}^{+\infty} E_{IR}(t-t')S(t')dt' \tag{3}$$

For the result presented in Fig. 1(a), we assumed that the fs IR pulse has Gaussian duration of 150 fs FWHM and that the material system has two resonant IR transitions spaced by 40 cm^{-1}, each having a Lorentzian lineshapes of 24 cm^{-1} FWHM. In the radiated field, the instantaneous nonresonant response may be the dominant term, particularly so for metal substrates, less so for dielectric substrates. Therefore, it is critical to suppress the instantaneous nonresonant contribution to the extent possible. NRB suppression can be achieved by applying a time-delay between the fs IR and ps visible pulses. The second order polarization obtained by upconversion of the first order polarization by the time-delayed ps visible pulse is given by

$$P^{(2)}(t,\tau) \propto E_{vis}(t-\tau)P^{(1)}(t) \tag{4}$$

where τ is the time-delay between IR and visible pulses. The second order nonlinear polarization $P^{(2)}(t,\tau)$ can be Fourier transformed to $P^{(2)}(\omega,\tau)$ and the power spectrum of the SFG signal is given by

$$I \propto \left| P^{(2)}(\omega,\tau) \right|^2 = \left| \int_{-\infty}^{+\infty} P^{(2)}(t,\tau)\exp(i\omega t)dt \right|^2 \tag{5}$$

#126129 - $15.00 USD Received 29 Mar 2010; revised 29 Apr 2010; accepted 6 May 2010; published 14 May 2010

In the following, we will compare these SFG power spectra as a function of time-delay for three different ps visible pulse shapes; the 4f, étalon and inverted pulse shapes and for two different ps laser spectral resolutions. For the SFG simulations, we considered the case of two Lorentzian transitions (central frequencies of 2880 cm^{-1} and 2920 cm^{-1}) having the same amplitude and linewidths. These Lorentzian linewidths are 30 cm^{-1} FWHM for (e)-(g) and 12 cm^{-1} FWHM for (h)-(j). The fs IR pulse is assumed to be a Gaussian (150 fs FWHM) centered at 2900 cm^{-1} and the spectral bandwidths of the shaped ps visible were taken to be 24 cm^{-1} FWHM for (e)-(g) and 10 cm^{-1} for (h)-(j). In order to emphasize the dependence of NRB suppression on the ps pulse shape, we have introduced a large nonresonant contribution ($A_{NR} = 5$) with a relative phase shift φ_{NR} of $\pi/2$. We show the commonly used ps visible pulse shapes for 24 cm^{-1} bandwidth: the time-symmetric 4f pulse shape, Fig. 1(b), and the time-asymmetric étalon pulse shape, Fig. 1(c). The computed SFG spectra as a function of time-delay between the fs IR and the 24 cm^{-1} visible pulses for the 4f and étalon pulse shapes are given in Figs. 1(e) and 1(f), respectively. The general convention used here, and in the following section, is that the IR pulse arrives at t = 0, and the visible pulse can either be delayed to arrive later (corresponding to a positive delay) or earlier (corresponding to a negative delay). In all examples the IR power, molecular response function (S) and visible pulse power is kept constant. The resulting VSFG spectra are normalized, in order to be able to compare the resolution for different visible pulse shapes [(e) to (g) and (h) to (f)]. By introducing time delays, the 4f pulse shape suppresses the NRB and increases the SFG spectral resolution as the FID is more fully sampled, see Fig. 1(e). Importantly, the magnitudes of the signals as a function of delay are different for these pulse shapes, with the 4f shape falling most rapidly. This issue is discussed below. We also note that optimal NRB suppression for the 4f pulse shape occurs at a time delay corresponding to the first minimum in the sync function. As previously noted [9], optimum time-delay for a time-asymmetric étalon pulse is comparable with the IR pulse duration. The étalon pulse also suppresses the NRB but at the expense of reduced sampling of the resonant response at short time. It thus generally produces broader line shapes, as in Fig. 1(f). We note that for broader vibrational transitions (e.g. O-H, N-H stretch), NRB suppression with delayed étalon pulses may produce artificially broad lines and peak shifts. The same plots of the VSFG spectra are shown in panels (h) and (i), for narrower resonance linewidths 12 cm^{-1} and visible pulse bandwidths of 10 cm^{-1}. Again, it can be seen that the 4f pulse shape yields higher spectral resolution but at the expense of signal magnitude. The longest time delay, 3200 fs (*), corresponds to the zero in the sync function and, hence, the most symmetric lineshapes. However, the signal levels at this delay may be unacceptably small.

We now discuss the formation of 'inverted' time-asymmetric ps visible pulses using second harmonic generation (SHG) in a long nonlinear crystal having high group velocity mismatch. The theory of SHG and the effects of crystal length are well known [12,13]. Assuming exact phase matching at the pulse carrier frequencies and small conversion efficiencies (less than few percent), the fundamental pulse does not suffer losses upon propagation through the nonlinear crystal, thus producing, due to the walk-off between the second harmonic (group velocity v_2) and the fundamental (group velocity v_1), time-symmetric square-top ps pulses. In this ideal case, the pulse duration is determined by the crystal length (L) and the group velocity mismatch, approaching a value of $L/\left|v_1^{-1} - v_2^{-1}\right|$. In reality, the fundamental pulse does deplete due to high conversion. In a nonlinear crystal where both the conversion efficiency and the group velocity mismatch are high, SHG yields a long time-asymmetric pulse whose intensity increases exponentially with time, as in Fig. 1(d). For our experiments, we specifically chose $LiNbO_3$ as the nonlinear crystal since it has very high group velocity mismatch (300 fs/mm at 1300 nm) combined with good conversion efficiency.

#126129 - $15.00 USD Received 29 Mar 2010; revised 29 Apr 2010; accepted 6 May 2010; published 14 May 2010

For this inverted pulse shape, a positive time delay (peak of the pulse arriving after the resonant IR pulse) is essential in order to preferentially sample the resonant response, as shown in Fig. 1(g) and 1(j). At short time delay (250 fs, solid black), the strongest contribution to the SFG signal comes from nonresonant response (dashed), essentially reproducing the Gaussian fs IR pulse spectrum. At longer time delays, the inverted pulse minimally samples the nonresonant response while maximally sampling the resonant response. This SFG spectrum has spectrally resolved vibrationally resonant transitions with very small contributions from the NRB.

In the BB-SFG approach, the time delayed inverted pulse provides spectral resolution and NRB suppression similar to the time-delayed 4f pulse shape. The signal levels as function of time delay, however, behave quite differently. At the highest spectral resolution (3200 fs), the 4f signal level in (h) is more than 5 times smaller than the inverted signal in (j). At 1800 fs time delay, closely resembling our experimental conditions, the inverted pulse shape is expected to be superior in both resolution and signal magnitude. Ultimately, the choice of optimal ps pulse shape will depend on the specific characteristics of the material system. In the following, we demonstrate the utility of the inverted ps pulse shape for applications in vibrational spectroscopy.

3. Experiment

Our BB-SFG setup, depicted in Fig. 2, is based on Ti:sapphire high power fs laser system which was described in detail elsewhere [14]. Briefly, 80 fs, 800 nm pulses at a 1 kHz repetition rate are produced by fs Ti:sapphire regenerative amplifier (Coherent, Legend). Approximately 400 μJ of the Ti:Sa fundamental is used to pump a fs optical parametric amplifier (LightConversion TOPAS), producing signal (**S,** 1300 nm) and idler (**I**, 2080 nm) outputs. Signal and idler are separated and recombined for non-collinear difference frequency mixing in a 1.2 mm $AgGaS_2$ crystal, producing broad bandwidth (~150 cm^{-1} FWHM) fs IR pulses centered around 2900 cm^{-1}. As shown in Fig. 2, the residual signal **S** (~30 μJ) emerging from the $AgGaS_2$ crystal is spatially separated from the idler **I** and DFG fs IR signals. The residual **S** is used to produce narrow bandwidth 'inverted' ps visible pulses (centered at ~650 nm) by second harmonic generation in a long $LiNbO_3$ crystal (either 1 or 2 cm, $\theta = 58.9°$).

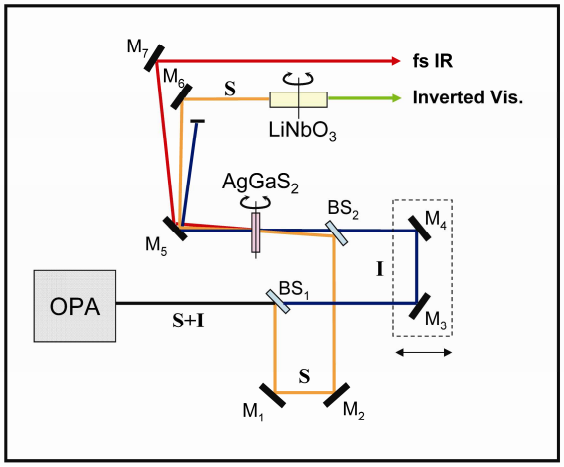

Fig. 2. Schematic diagram of the optical system layout for broad band fs IR generation and simulataneous narrowband ps visible pulse generation. A fs OPA produced signal (**S**) and idler (**I**) pulses. These are different frequency mixed in a thin $AgGaS_2$ crystal, producing fs IR pulses. The residual signal (**S**) is doubled in a long $LiNbO_3$ crystal, producing a narrowband visible pulse having an inverted time-asymmetric profile, due to the SHG process.

#126129 - $15.00 USD Received 29 Mar 2010; revised 29 Apr 2010; accepted 6 May 2010; published 14 May 2010

The synchronized fs IR pulses and ps visible pulses are spatially and temporally overlapped at the horizontal sample surface. The incidence angles for visible and IR beams are ~62° and ~60°, respectively, from surface normal. The beams are focused using two lenses, (f = 50mm, CaF_2 for IR and f = 25mm, BK7 for visible). For systems of biological interest, optical damage by intense fs laser pulses is a concern. Low laser pulse energies at the sample were implemented: ~1.7 μJ/pulse for the fs IR and ~3 μJ/pulse for the ps visible. Large spot sizes, 250 μm for the IR and 150 μm for the visible, we used in order to further minimize potential damage at the sample. The polarization of the visible was controlled by Berek's polarization compensator (BC) while the polarization of IR was set to be vertical using a periscope. The SFG signal from the sample surface was recollimated and frequency filtered, passing through a 300 mm monochromator (Acton Spectra-Pro 300i) before being detected by a cooled (−40 °C) nanosecond gated intensified CCD camera (Princeton Instruments PI-MAX: 1024 Unigen II, 1024 × 256 pixels). We used a 200 nanosecond gate to minimize background light. For data acquisition, 8 pixels horizontal binning on the CCD chip was applied to further reduce noise. Data collection times for SFG spectra ranged from 2 to 9 min, depending on SFG signal level (2 min for SAM on gold, 9 min for the 1-octanol-air water interface and LB films). To optimize the resonant signals and simultaneously suppress the NRB, IR-visible time delays of ~1.5 ps were used, as described in the theory section.

The time profile of the 'inverted' visible pulse was measured via SFG cross correlation using the nonresonant signal from a GaAs crystal interface. The time delay was controlled by a Newport MFN linear stage with 0.1 μm accuracy. The cross correlation signal was detected using a 1P28 photomultiplier tube (PMT) and amplified with a gain of 25 by a preamplifier coupled through 470 pf into a boxcar integrator (Stanford Research Systems).

1-dodecanethiol coated SAM on gold was prepared by incubating a clean gold slide in an ethanoic thiol solution (24 hours at room temperature), followed by rinsing with ethanol to remove excess thiols from the surface. A monolayer of 1,2-dimyristoyl-*sn*-glycero-3-phosphocholine (DMPC, Avanti Polar Lipids) was prepared on glass by standard Langmuir-Blodgett (LB) methods. These samples were dried for at least 24 hours in a N_2 purged desiccator before SFG measurement. A 1 mM 1-octanol (BDH, 95%) solution was prepared using Milli-Q water (resistivity 18 MΩ.cm, total organic carbon <10 ppb). For SFG measurement, the solution was kept for 10 min in a clean Teflon Petri dish to form an equilibrium 1-octanol monolayer at the air-water interface.

#126129 - $15.00 USD Received 29 Mar 2010; revised 29 Apr 2010; accepted 6 May 2010; published 14 May 2010

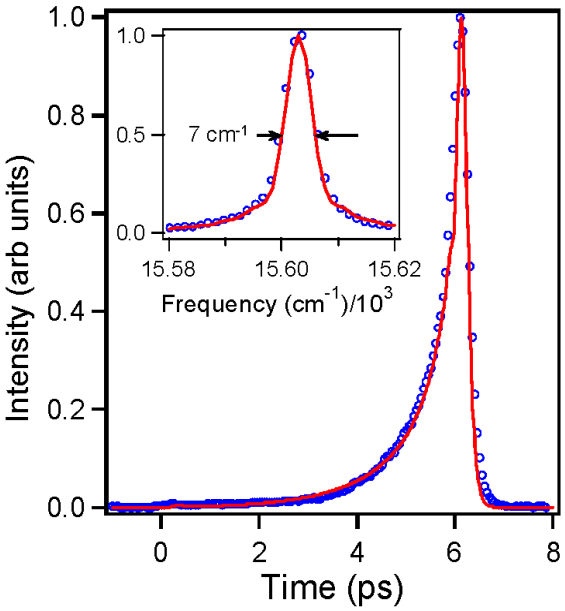

Fig. 3. The experimental cross correlation, shown as open blue circles, of the time-asymmetric pulse from a 2 cm $LiNbO_3$ crystal. The thin red line shows the independent result from a calculation (no adjustable parameters). The inset shows the measured visible pulse spectrum, as blue circles, and, as the red line, the Fourier transform power spectrum of the computed deconvolved cross correlation shown in the main figure. For details, see the text.

4. Results and discussion

In Fig. 3 we present the measured fs IR – ps visible cross correlation and, inset, the measured spectrum of visible ps pulse. Data for the case of a 2 cm $LiNbO_3$ SHG crystal are shown as open blue circles. The solid red lines are obtained by independent calculation of the SH generation process using SNLO v.48, plane-wave short pulse mixing (A.V. Smith, AS-photonics, Albuquerque, NM). There were no adjustable parameters – the red lines are not a fit. The computed spectrum corresponds to Fourier transformation of the time profile. The agreement between experiment and calculation is excellent. It can be seen that the long $LiNbO_3$ SHG crystal produces a well characterized 'inverted' pulse shape. The cross correlation and spectrum for SHG using a 1 cm $LiNbO_3$ crystal (not shown) are also in agreement with the computed SNLO results. The spectral line width of the visible pulse (~7 cm^{-1} and ~13 cm^{-1} for 2 cm and 1 cm crystals, respectively) is well suited to high quality spectroscopic resolution in the C-H stretch region for most surface molecular systems. In the cross correlation shown in Fig. 3, the signal rises from less than 10% of the maximum intensity to the maximum value in approximately 2.5 ps, indicating substantial NRB suppression is expected, as depicted in Fig. 1(g) and 1(j).

Due to pump depletion and back-conversion, SHG in a long crystal can in principle lead to pulse shapes and spectra which depend on radial position (i.e. intensity) within the Gaussian spatial mode of the output pulse. In order to check this, we scanned a pinhole over the collimated SHG beam emerging from the long $LiNbO_3$ crystal and recorded spectra as a function of spatial position with the laser spot. In our case, no variation of the pulse spectrum with radial position was observed.

#126129 - $15.00 USD Received 29 Mar 2010; revised 29 Apr 2010; accepted 6 May 2010; published 14 May 2010

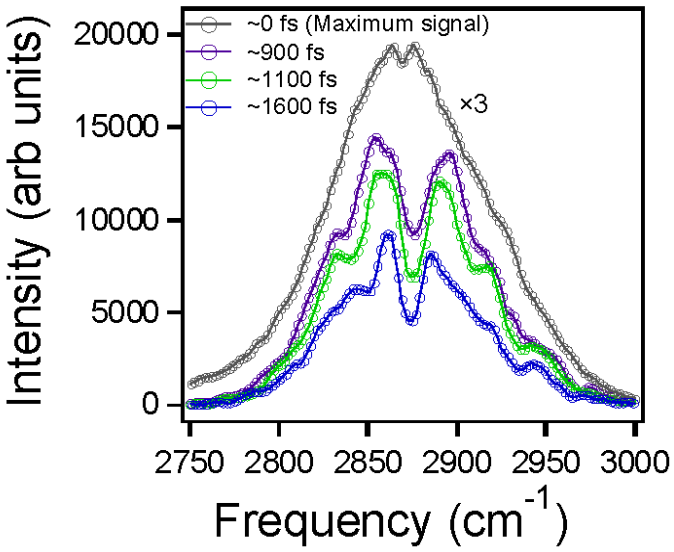

Fig. 4. BB-SFG spectra of 1-dodecanethiol SAM on gold for different IR and visible time-delays, recorded using PPP polarization. A time delay between the IR and visible is applied to minimally sample the NRB from gold and maximally sample the resonant signal.

SFG spectra of 1-dodecanethiol SAM on gold of C-H stretch region are shown in Fig. 4. For these spectra, inverted pulses from 1 cm $LiNbO_3$ crystal were used. The time delay of ~0 fs is defined as the delay position which gives maximum SFG signal, essentially reproducing the Gaussian IR spectrum as described in Fig. 1. Introducing a time-delay between the IR and inverted visible pulses, the vibrational C-H transitions appear as negative going dips in the Gaussian IR envelope [15]. The NRB signal from gold is a few orders of magnitude larger than calculated spectra in Fig. 1. It is therefore not feasible to completely suppress it. SFG spectra were recovered by dividing the SFG spectrum of SAM on gold by the NRB signal from bare gold, as is shown in Fig. 5(a). In order to record VSFG spectra in a reproducible manner, it is important to be able to set and control the spectrum of the visible pulse. In our scheme this is defined by the signal wavelength, and the phase matching angle of the long $LiNbO_3$ crystal. In this paper we discuss mainly VSFG in the C-H stretch region around 2900 cm^{-1}, however, in order to probe different vibrational transitions adjacent to alkyl C-H stretch, it will be required to tune the IR frequency. This involves changing the signal and idler wavelengths which in turn requires tuning of the generation of the visible pulse.

#126129 - $15.00 USD Received 29 Mar 2010; revised 29 Apr 2010; accepted 6 May 2010; published 14 May 2010

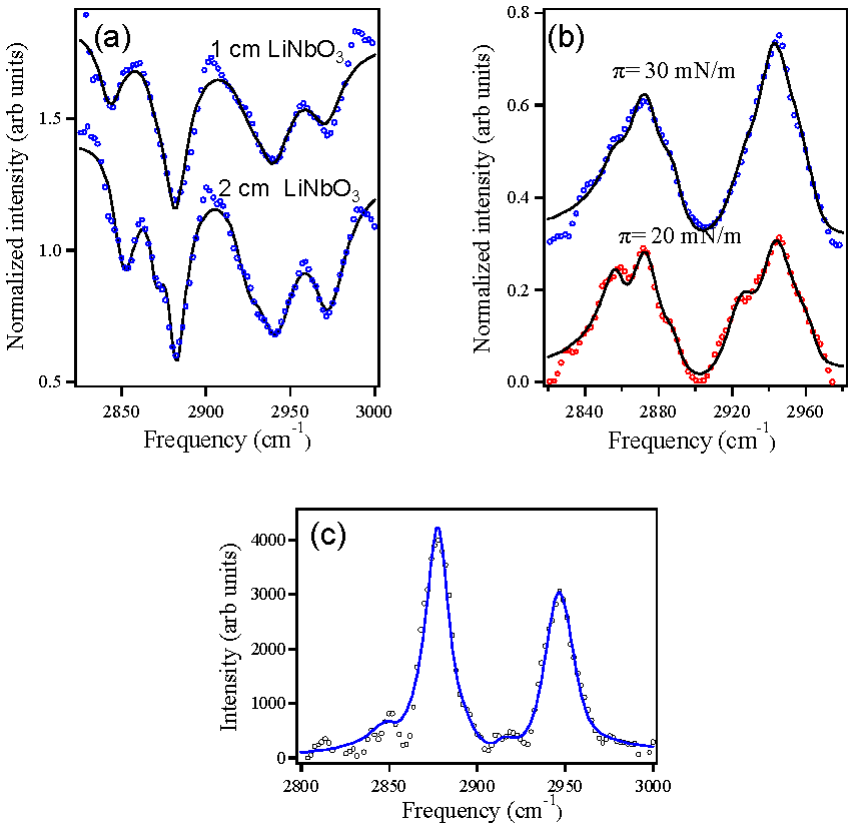

Fig. 5. BB-SFG spectra of: (a) 1-dodecanethiol SAM on gold using PPP polarization; (b) LB monolayer of DMPC under SSP polarization at two surface pressures; (c) 1-octanol air-water interface under SSP polarization. These results confirm the utility of the inverted pulse BB-SFG scheme.

For two different 'inverted' visible pulses (1 cm and 2 cm $LiNbO_3$), SFG spectra of 1-dodecanethiol SAM on gold were recorded and the results are shown in Fig. 5(a). The spectra in the C-H stretch region are dominated by three transitions which can be assigned to the CH_3 symmetric stretch $\nu(r^+)$ = 2882 cm^{-1}, the Fermi resonance of r^+, $\nu(r_{FR}^+)$ = 2940 cm^{-1} and the CH_3 asymmetric stretch, $\nu(r^-)$ = 2970 cm^{-1}. Due to the *gauche* conformation of the SAM monolayer, two weak CH_2 transitions are observed that are centered at 2850 cm^{-1} (symmetric stretch, d^+) and 2919 cm^{-1} (asymmetric stretch, d^-). All the spectra were fitted using a standard multi-Lorentzian approximation [8]. These spectra are in good agreement with the reported SFG spectra of similar SAM on gold surfaces [15]. The SFG spectrum produced with inverted visible pulses from 2 cm $LiNbO_3$ crystal show higher spectral resolution, resolving the CH_2 asymmetric stretch adjacent to the terminal CH_3 group ($\nu(d_\omega^+)$ = 2868 cm^{-1}) in the d^+ band. This clearly demonstrates the capability of the inverted pulse BB-SFG approach for resolving finer features of vibrational spectra at interfaces.

The SFG spectra for a LB monolayer of DMPC are shown, at two different surface pressures (20 and 30 mN/m), in Fig. 5(b). Four main transitions are seen and are attributed to d^+ (2855 cm^{-1}), r^+ (2875 cm^{-1}), d^- (2920 cm^{-1}) and r_{FR}^+ (2942 cm^{-1}). Qualitatively, the increasing of the intensity of the CH_3 stretch transitions (r^+ and r_{FR}^+) relative to those of the CH_2 (d^+ and d^-) stretch transitions shows the closer packing of monolayer upon increasing surface pressure in the liquid condensed phase of the isotherm. In Fig. 5(c), we show the SFG

#126129 - $15.00 USD Received 29 Mar 2010; revised 29 Apr 2010; accepted 6 May 2010; published 14 May 2010

spectrum for well known model system of 1-octanol at the air-water interface [16]. The two strong transitions are assigned to r^+ (2879 cm^{-1}) and r_{FR}^+ (2944 cm^{-1}) and the two weak transitions are attributed to d^+ (2850 cm^{-1}) and d^- (2916 cm^{-1}), showing good agreement with prior studies. The results of these three surface studies show that the present 'inverted' pulse scheme is very comparable to other BB-SFG schemes.

5. Conclusion

We have presented a BB-SFG arrangement based on a single OPA system whose output is used to produce both broad band fs IR and an 'inverted' narrowband ps visible pulse. Second harmonic generation from a long nonlinear crystal having high group velocity mismatch is demonstrated to be a good approach for generating narrow band visible pulses with a time-asymmetric pulse profile which rise exponentially over a couple of ps, efficiently suppressing the electronic nonresonant background. Varying the time delay between the fs IR and the inverted visible pulse can be used to achieve good spectral resolution while minimizing contributions from the nonresonant background signal. This is achieved without significant artificial line broadening or peak shifting. The time delay between IR and visible pulses can be used as a variable to trade off spectral resolution vs. signal intensity. At the time delays used in these experiments (~1500 fs), we expect, as shown in Fig. 1, that the inverted pulse scheme will have both better spectral resolution and high signal levels than either the 4f or étalon. Finally, this approach makes very efficient use of fs Ti:Sa amplifier pulses, as no additional 800 nm pulse is required to generate the narrowband ps visible pulse.

#126129 - $15.00 USD Received 29 Mar 2010; revised 29 Apr 2010; accepted 6 May 2010; published 14 May 2010